PNAS RESEARCH ARTICLE | GENETICS OPEN ACCESS

A rare germline BMP15 missense mutation causes hereditary ovarian immature teratoma in human

Yakun Liu[a,1], Hongwei Fan[a,1], Xi Kang[b], Yuntao Hao[a], Na Wang[c], Hui Zheng[d,2], Yan Li[c,2], and Shan Kang[a,2]

Edited by Chun Peng, York University, Toronto, ON, Canada; received June 21, 2023; accepted January 11, 2024 by Editorial Board Member Matthew P. Scott

Ovarian immature teratomas (OITs) are malignant tumors originating from the ovarian germ cells that mainly occur during the first 30 y of a female's life. Early age of onset strongly suggests the presence of susceptibility gene mutations for the disease yet to be discovered. Whole exon sequencing was used to screen pathogenic mutations from pedigrees with OITs. A rare missense germline mutation (C262T) in the first exon of the BMP15 gene was identified. In silico calculation suggested that the mutation could impair the formation of mature peptides. In vitro experiments on cell lines confirmed that the mutation caused an 84.7% reduction in the secretion of mature BMP15. Clinical samples from OIT patients also showed a similar pattern of decrease in the BMP15 expression. In the transgenic mouse model, the spontaneous parthenogenetic activation significantly increased in oocytes carrying the T allele. Remarkably, a mouse carrying the T allele developed the phenotype of OIT. Oocyte-specific RNA sequencing revealed that abnormal activation of the H-Ras/MAPK pathway might contribute to the development of OIT. BMP15 was identified as a pathogenic gene for OIT which improved our understanding of the etiology of OIT and provided a potential biomarker for genetic screening of this disorder.

ovarian immature teratoma | BMP15 gene | pathogenesis | hereditary

Significance

We identify a rare germline missense mutation in the BMP15 from two pedigrees with OIT. Also, we found that some variant carrying mice develop a teratoma phenotype. Our findings demonstrate that rare mutations in the BMP15 may be the causative variant of human hereditary OIT and provided a potential biomarker for genetic screening of this disorder.

Ovarian immature teratoma (OIT) is a rare malignant germ cell tumor with an estimated incidence rate of 3.4×10^{-7} (1), representing less than 1% of ovarian cancers and 20% of ovarian malignant germ cell tumors (2). Ovarian immature teratomas and mature teratomas are alike in many aspects, and clinically, they are differentiated mainly by histology. Compared to mature teratomas, immature teratomas contain varying amounts of immature tissues; the most commonly identified is the neuro-differentiated tissue. OIT has a specific age incidence, mainly occurring in women under the age of 30, and rarely occurs after menopause (3). Due to its rarity, limited clinical information is available, and there is a lack of reliable epidemiological data, and as a result, the etiology of OIT is poorly understood. In contrast, the origin of ovarian mature teratomas (OTs) has been well studied. These tumors are thought to arise from a single ovarian germ cell via parthenogenesis after the first meiotic division (4, 5). This hypothesis is also supported by the high proportion of spontaneous ovarian teratomas occurring in some mouse strains with inherited mutation (*c-mos*-null and LT/Sv) (6–9). The origins of OIT are thought to be similar to that of OTs based on several observations, namely, the presence of normal karyotypes (46, XX) in OIT patients (10, 11) and the extremely low mutation rate (3) and extensive genomic loss of heterozygosity in OIT (12, 13). However, direct data to support this model are still absent.

Here, we report two pedigrees with OIT. A rare germline missense mutation, C262T, in exon 1 of the bone morphogenetic protein 15 (*BMP15*) gene located on the X chromosome was found to be a pathogenic variant for OIT. BMP15, an oocyte-derived growth and differentiation factor, plays a crucial role in mammalian reproduction, regulating species-specific fecundity, ovarian follicular somatic cell differentiation, and oocyte quality (14–17). In humans, *BMP15* variants are associated with different ovarian phenotypes, including premature ovarian insufficiency (POI) and polycystic ovary syndrome (PCOS) (18, 19). To validate the pathogenic effect of the C262T mutation in OIT, we generated genetically engineered mice (C57BL/6J) harboring orthologous missense variants by CRISPR–Cas9 genome editing. The oocytes of genetically engineered female mice displayed prominent parthenogenetic activation and produced a phenotype similar to that in human OTs. Oocyte-specific RNA-seq revealed that H-Ras and MEK1 overexpression might be responsible for the development of the disease.

Author affiliations: [a]Department of Gynecology, Fourth Hospital, Hebei Medical University, Shijiazhuang 050011, China; [b]Department of Surgery, Fourth Hospital, Hebei Medical University, Shijiazhuang 050011, China; [c]Department of Molecular Biology, Fourth Hospital, Hebei Medical University, Shijiazhuang 050011, China; and [d]Nanjing Personal Oncology Biotechnology Co., Ltd., Nanjing, Jiangsu 211103, China

Author contributions: Y. Liu, H.Z., Y. Li, and S.K. designed research; Y. Liu and H.F. performed research; Y. Liu, H.F., X.K., H.Z., Y. Li, and S.K. contributed new reagents/analytic tools; X.K., Y.H., N.W., H.Z., Y. Li, and S.K. analyzed data; and Y. Liu wrote the paper.

The authors declare no competing interest.

This article is a PNAS Direct Submission. C.P. is a guest editor invited by the Editorial Board.

[1]Y. Liu and H.F. contributed equally to this work.

[2]To whom correspondence may be addressed. Email: zhenghui@personaloncology.cn, lykx1962@163.com, or ksjq62cn@sina.com.

This article contains supporting information online at https://www.pnas.org/lookup/suppl/doi:10.1073/pnas.2310409121/-/DCSupplemental.

Published March 1, 2024.

Results

Genetic Alterations in Hereditary Ovarian Immature Teratoma. Whole-exome sequencing analysis revealed that all affected women carried a rare missense mutation at position 262 (c.C262T) in exon 1 of the *BMP15* gene, which was confirmed via Sanger sequencing (Fig. 1*C*). This C262T variant was present in two affected individuals in pedigree 1 and absent in the two unaffected females (II-2, III-2). In contrast, the same variant was present in all immediate family members in the second and third generations of pedigree 2, indicating paternal transmission (Fig. 1*A*). The C262T mutation was reported with an allele frequency of 6.478×10^{-6} in the gnomAD database and was not present in the 1000 Genomes Project databases or the ESP database. This mutation was not found in the other five cohorts. Although not all carriers of the variant in pedigree 2 showed symptoms, considering the extremely low population frequency of this variant and its absence in all other controls, we speculated that the C262T variant might be involved in the pathogenesis of hereditary OIT. In addition, the two pedigrees indicate that hereditary OIT may be a rare disorder with X-linked dominant inheritance that exclusively affects heterozygous females.

C262T Variant Affects the Protein Expression of BMP15. The C262T mutation causes a substitution of the arginine (R) residue at position 88 of *BMP15* with a cysteine (C) residue. The R88 residue is located in the pro-region of the BMP15 protein and is extensively conserved across mammals (Fig. 1*D*). The change was also predicted to be damaging by multiple in silico algorithms, including SIFT and PolyPhen2. Furthermore, we compared the structures of the mutated BMP15 and the wild-type protein by rmsd. The score was 7.065, indicating that the R88C single mutation does alter the three-dimensional structure of BMP15. The predicted structure indicated that substantial switching of an alpha helix into a random coil is caused by this mutation (Fig. 1*F*). Theoretically, the new cysteine generated by the C262T mutation could form a new disulfide bond and could corrupt the original structure of the proprotein. Since no purified protein samples are available for crystal diffraction, we tried the in silico predictions. Two sets of individual software were used. One is the scratch protein predictor (https://scratch.proteomics.ics.uci.edu/) (20), and the other is Cyscon (https://www.csbio.sjtu.edu.cn/bioinf/Cyscon/) (21). Both in silico predictions suggested the formation of a new disulfide bond between the cysteine generated by the C262T variant and the cysteine at position 13 of the protein sequence.

Variants in the pro-region of BMP15 are able to modulate the expression and activity of mature proteins (15, 22). Therefore, we first tried to determine whether this C262T mutant can affect the protein level of mature and secreted BMP15. Wild type and C262T mutated BMP15 were overexpressed in same numbered 293T cells. The secreted proteins were purified from the culture medium and were analyzed by western blot. The result showed a significant reduction (84.7%) of secreted BMP15 in C262T-transformed HEK293T cells (Fig. 2*A*). Immunohistochemical staining showed that wild-type BMP15 was mainly expressed in the cytoplasm of oocytes and granulosa cells in normal ovarian tissues and in the three germ layers in immature teratomas. Notably, the expression level of the mature BMP15 protein was significantly decreased in immature teratomas carrying the C262T mutation (Fig. 2 *B*–*D*). These results suggest that the C262T mutant could lead to a substantial reduction in BMP15 secretion.

Parthenogenetic Activation of Oocytes in Mice with the *BMP15* C262T Mutation. It is a well-accepted hypothesis that immature ovarian teratomas originate from the asexual development or parthenogenesis of oocytes, stimulated by unknown triggers (4). To assess whether the *BMP15* C262T variant can induce parthenogenesis to produce OIT in vivo, we calculated the parthenogenesis activation rates of female mouse oocytes of three different genotypes (CC, CT, and TT). Ovaries from 4-wk-old female mice from the same litter were collected after genotyping by Sanger sequencing. Oocytes were isolated and assessed under a microscope for parthenogenetic activation. Approximately a total of 100 oocytes were used for each genotype. Parthenogenetic activation was assessed by the evaluation of oocyte morphology; oocytes with two pronuclei (Fig. 3*A*) or two polar bodies (Fig. 3*B*) and the appearance of two-cell structures (Fig. 3*C*) were considered to indicate parthenogenesis (23). We observed that the proportion of parthenogenetic activation was 8.4% in mice with the CC genotype, 32.5% in mice with the CT genotype, and 51.3% in mice with the TT genotype (Fig. 3*G* and *SI Appendix*, Table S2). Histological analysis of mouse ovarian sections (H&E staining) also showed that the oocytes in the ovarian tissue of the mice with the CT and TT genotypes more often exhibited 2-pronuclei (Fig. 3*D*), 2-polar body (Fig. 3*E*) and two-cell (Fig. 3*F*) phenotypes than those of the mice with the CC genotype. These results indicate that the *BMP15* C262T variant significantly stimulates parthenogenic activation.

Oocyte-Specific RNA Sequencing Revealed MAPK Activation by *BMP15* Mutation. To understand the potential mechanism of tumorigenesis due to the C262T variant, we performed RNA-seq to analyze the transcriptomes of mouse oocytes from three different genotypes. Because there are an overwhelming number of granulosa cells in the ovary, the actual differential signals in the oocytes will be flooded by noise from the granulosa cells when using bulk sequencing. Therefore, we used an oocyte-specific sequencing. After genotyping, 4-wk-old mice with the same genotype from the same litter or separated litter but with the same father and maternally the same litter were used. After the stimulation by pregnant mare serum gonadotropin (PMSG) and human chorionic gonadotropin (hCG), oocytes were isolated and collected by microdissection. About 140 to 200 oocytes were collected for each genotype. Oocytes with the same genotype were pooled for the sequencing. The results showed 1,815 differentially expressed genes (DEGs) between the CC and CT genotypes and 6,548 DEGs between the CC and TT genotypes. Among all the DEGs, 1,082 genes were common between the two groups (Fig. 4*A*). There was a significant difference in the expression pattern of the CC genotype and the other two genotypes (Fig. 4*B*). Kyoto Encyclopedia of Genes and Genomes (KEGG) pathway enrichment analysis revealed that the DEGs were significantly enriched in long-term depression, cholinergic synapse, relaxin signaling, and apoptosis pathways.

Notably, *H-Ras* and *MEK1* were simultaneously enriched in these pathways. The expression of H-Ras in mouse oocytes with the CT and TT genotypes was 3.2-fold and 8.3-fold higher than that in oocytes with the CC genotype. Moreover, the expression of MEK1 in oocytes carrying CT or TT mutations was 3.9-fold and 5.8-fold higher than that in oocytes carrying the CC genotype, respectively (Fig. 4*C*). Therefore, we speculate that the mutation of *BMP15* may activate the H-Ras/MAPK signaling pathway, resulting in abnormal oocyte proliferation and the incidence of ovarian teratoma. We examined the protein levels of H-Ras, MEK1, and p-MEK1 by immunohistochemical staining. The results confirmed that H-Ras and MEK1 levels were significantly higher in mouse oocytes with CT and TT genotypes than in those with the CC genotype and were negatively correlated with the expression of BMP15 (Fig. 4*D*).

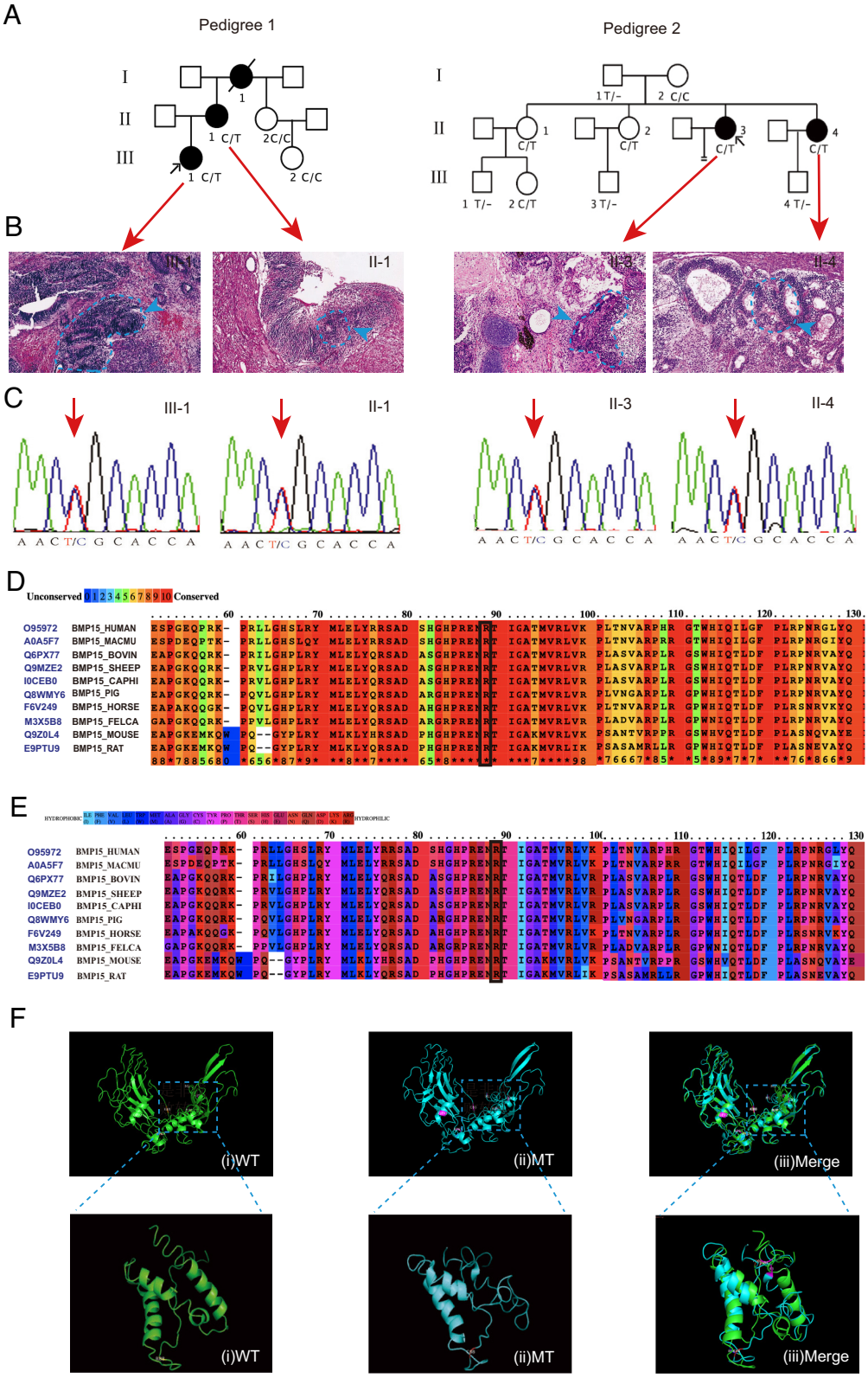

Fig. 1. Pathogenic mutant in familial ovarian immature teratoma. (*A*) Cases from two pedigree of OIT and their corresponding genotypes of *BMP15*. (*B*) Pathological diagnosis of corresponding patients. Blue dash-circled areas and arrowheads indicate two to three germ layer-derived tissues in the tumor tissue; neural components and neuroglia in the ectoderm; and the neuroepithelium is connected into pieces in a daisy doughnut or irregular glandular shape. (*C*) Sanger sequencing results of corresponding patients. (*D*) Conservation of Arg 88 across various species. (*E*) Hydrophilicity of Arg 88 across various species. (*F*) Predicted structural change of c.C262T (MT) mutated *BMP15*.

C262T Mutant Causes Overgrown Ovary and Ovarian Teratoma in Mice. We examined the ovary development of genetically engineered mice at 4 wk, 8 wk, 12 wk, and 6 mo of age. No significant changes were observed at weeks 8 and 12 (Fig. 4 *E, i, Left*). However, substantial differences were found at month 6 (Fig. 4 *E, i, Right*), a time point when the normal ovary will

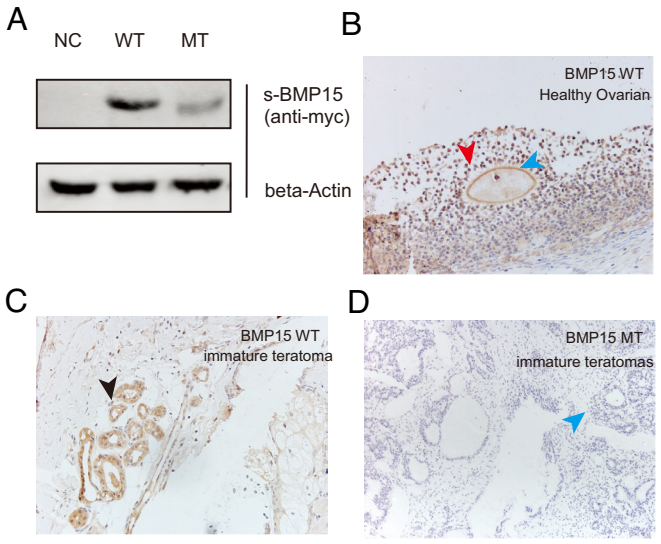

Fig. 2. C262T mutant affects the protein expression of BMP15. (*A*) Wild type and C262T mutated BMP15 were overexpressed in HEK293 cells. Amounts of secreted BMP15 (s-BMP15) were compared by western blot. Signal intensity was semi-quantified using ImageJ with the arbitrary unit ($P < 0.05$). (*B*) The general BMP15 protein level in a healthy ovarian, BMP15 was highly expressed in both granulosa cells (red arrow) and oocytes (blue arrow) of healthy ovaries; (*C*) Wild-type BMP15 in sporadic ovarian immature teratoma, BMP15 is highly expressed in the follicular epithelium of tumors (black arrow). (*D*) C262T variant in familial ovarian immature teratoma. The expression level of the mature BMP15 protein was significantly decreased in immature teratomas carrying the C262T mutation (blue arrow).

generally be dysfunctional, and few active oocytes could be found. Twenty mice from each group (CC and CT) were examined. Remarkably, we found that the average size of the ovaries in the CT mice was over onefold larger than that of wild-type mice (Fig. 4 *E, ii* and *SI Appendix*, Fig. S1). We also found that the average numbers of follicles per slicing section in the CT mice were much higher than that in the wild type, particularly the primary and the secondary follicles (Fig. 4 *E, iii* and *SI Appendix*, Table S4). Notably, one abnormal ovary was found among the 20 CT genotype ovaries. Pathological examination revealed an ovarian teratoma in this abnormal ovary. A digestive tract structure composed of layers of epithelial cells was found inside the ovary, where only granulosa cells and oocytes should be seen (Fig. 4*F*). We also inspected the protein levels of BMP15, H-Ras, and MEK1 and the phosphorylation status of MEK1 in the teratoma. Again, the proteins in the MAPK pathway showed a high level of expression and activation (Fig. 4*G*).

Discussion

OIT was first described in 1960 by Thürlbeck and Scully (24), but little is known about its genetic underpinnings. In the present study, we confirmed that familial OIT could be a hereditary tumor and identified *BMP15* as a candidate causative gene for the disease. The specific variant (C262T) identified in the study did not show a complete penetrance, which is common for mutations involved in hereditary tumors, such as *BRCA1/2* in ovarian cancer (25). Among the two families studied, all patients are heterozygous carriers. Therefore, we consider OIT to be an X-linked dominant genetic disorder. Since BMP15 is a specific growth factor secreted by oocytes, it affects only female carriers.

OIT is a genetically distinct tumor among the broad spectrum of human cancers, characterized by its essentially diploid genome, lack of somatic mutations, and extensive allelic imbalance (3, 12, 13). It is believed that the cellular origin and pathogenesis of OIT is similar to that of OTs, originating from asexual development or parthenogenesis of primary oocytes triggered by unknown factors. However, evidence to validate this hypothesis is lacking (10, 26, 27). Unlike OIT pathogenesis, the pathogenesis of OTs has been studied to a

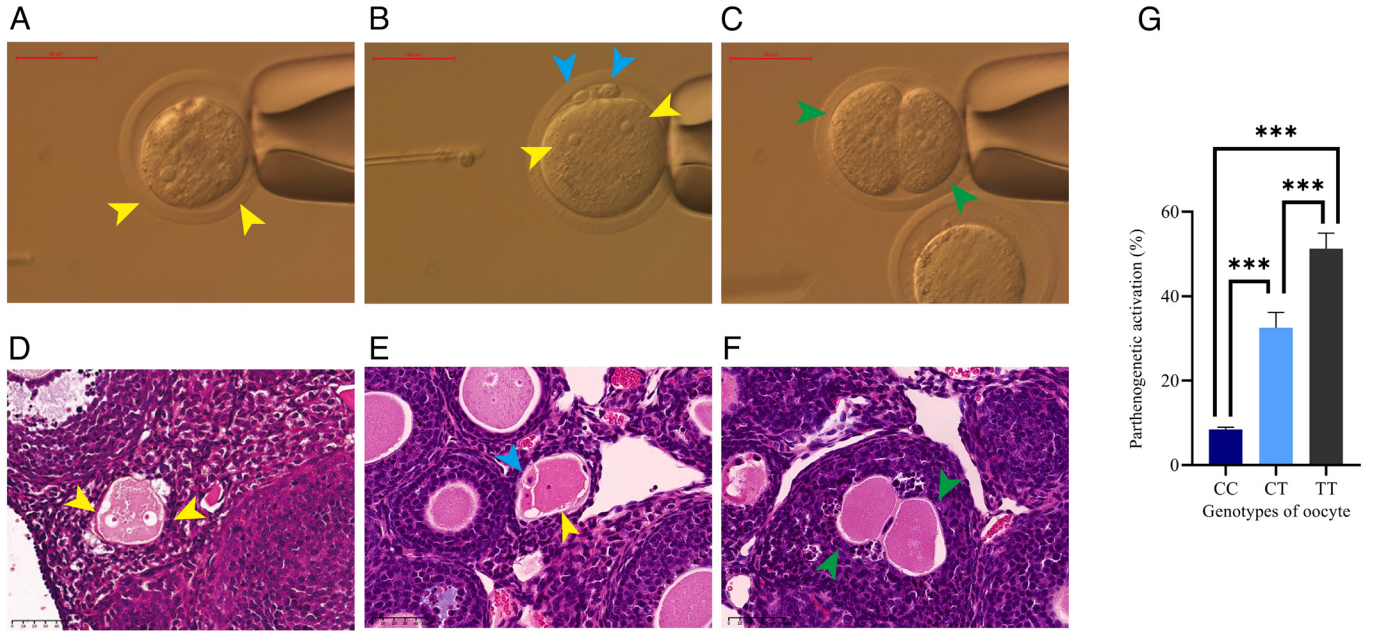

Fig. 3. C262T mutant significantly stimulates parthenogenetic activation of oocytes. Oocytes were collected from genetically engineered mice harboring the orthologous of BMP15 wild type or C262T variants. Superovulation was induced at 4 wk of age mice. Ten ovaries were assessed from each genotype. The parthenogenetic activation in oocyte was assessed by morphological changes (panel *A–C*) or histological stain (panel *D* and *E*). (*A*) Two pronucleus were seen in oocyte with spontaneous parthenogenetic activation (yellow arrowhead); (*B*) two pronucleus and two polar bodies were seen in oocyte with spontaneous parthenogenetic activation (yellow and blue arrowheads, respectively); (*C*) Two-cell (green arrowheads) was seen with spontaneous parthenogenetic activation; (*D*) The oocytes appear to have two pronucleus in the HE section (yellow arrowhead); (*E*) Two polar bodies and one pronucleus appear in the oocyte in the HE section (yellow and blue arrowheads, respectively); (*F*) Two-cell (green arrowheads) appeared in HE sections; (*G*) The percentage of parthenogenetically activated oocytes in different *BMP15* variants was counted under the Leica DMI3000B inverted biological microscope.

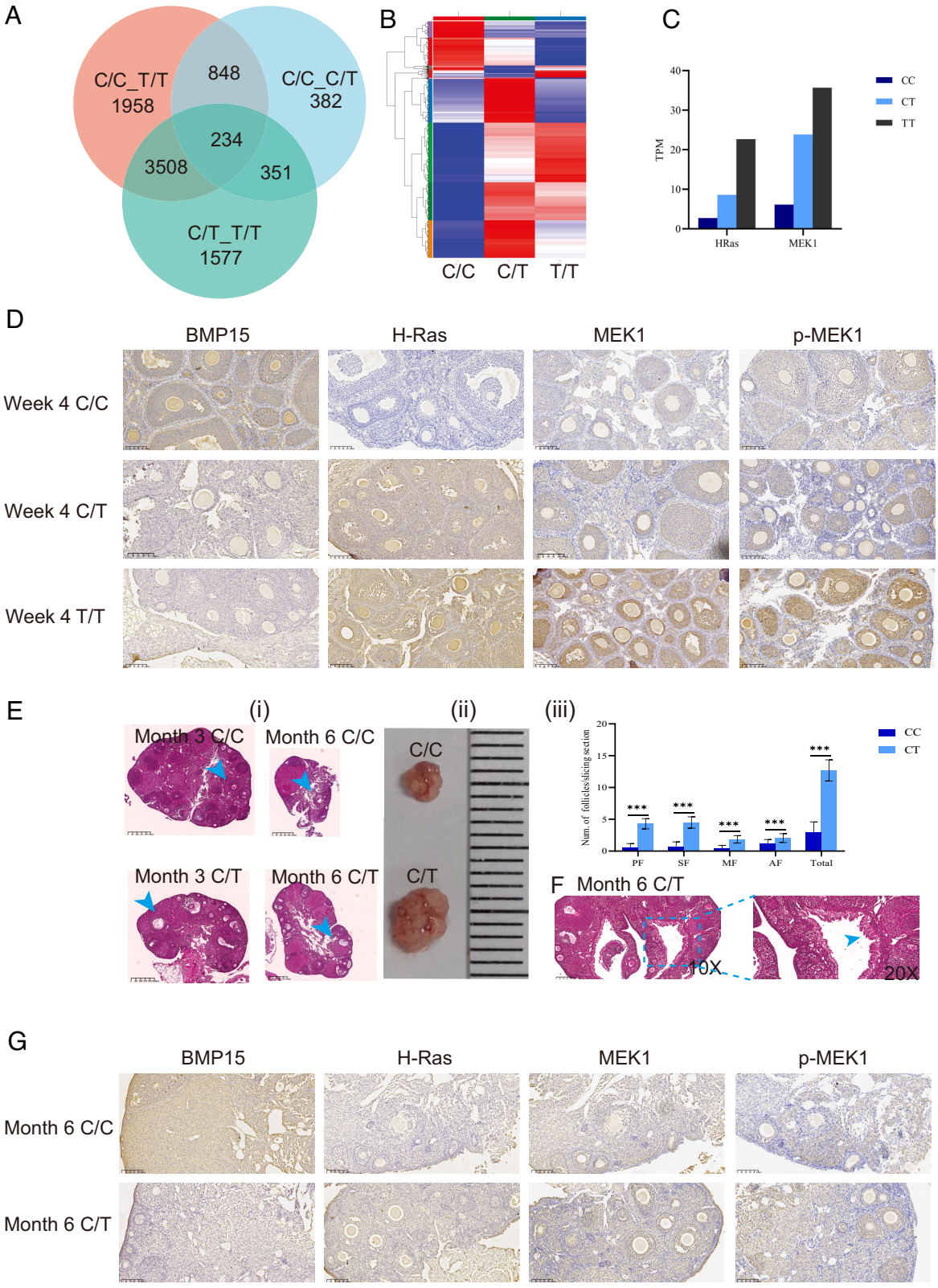

Fig. 4. H-Ras activated MAPK stimulate spontaneous activation of the oocytes and overgrown of the ovary. (*A*) Venn diagram showing the enriching strategy of oocytes specific RNA sequencing results. (*B*) Heat map showing the distinct diverse pattern of differential expressed genes in oocytes with wild-type or mutated BMP15. (*C*) H-Ras and MEK1 RNA levels in CC, CT, or TT type oocytes. (*D*) IHC stain showing the BMP15, H-Ras, MEK1, and p-MEK1 protein levels in CC, CT, or TT type ovarian tissues at week 4. (*E*) (*i*) Hematoxylin and eosin stain of ovarian tissues at the longest latitude section; blue arrowheads show follicles; (*ii*) the actual ovary size of CC and CT type at month 6; (*iii*) average counts of ovarian follicles per slicing section at month 6. PF, primary follicle; SF, secondary follicle; MF, mature follicle; AF, atretic follicle; *** indicates *P*-value < 0.001. (*F*) An ovarian teratoma in the CT type ovary. Blue arrowhead shows a digestive tract structure composed of layers of epithelial cells. (*G*) IHC stain showing the BMP15, H-Ras, MEK1, and p-MEK1 protein levels in a CC type healthy ovary and the CT type ovary with the teratoma at month 6.

certain extent. Congenital genetic defects have been found to be associated with OTs in mouse models. One example is that females in mouse strain LT/Sv showed a high frequency of spontaneous OTs arising from parthenogenetically activated follicular oocytes (8, 9, 28, 29). This spontaneous teratoma development was determined to be a polygenic trait, but the genes responsible have not yet been identified (28). Additionally, specific pathogenic genes for OTs have been identified in genetically modified mice. Two studies showed that *c-mos* deficiency could induce OTs, which was also characterized by the parthenogenetic activation of oocytes (6, 7). Other studies also showed that genes involved in regulating follicular cell and oocyte activity, including *Bcl-2*, FSH receptor, *Foxo3a*, *Inpp4b*, and *MC4R*, could induce OTs through different mechanisms (30–33).

In our study, we generated transgenic C57BL/6J mice carrying human *BMP15* C262T homologous missense mutation. The C262T variant in mice substantially increased the parthenogenetic activation rate of oocytes (Fig. 3*G*), and some variant-carrying mice developed teratomas in the sixth month (Fig. 4*F*). Naturally, the spontaneous parthenogenesis activation rate in C57BL/6J mice is 3% (28), and C57BL/6J mice did not show spontaneous teratoma (34). Therefore, the C262T variant should be the primary contributor to the substantial increase of parthenogenesis activation and formation of teratomas in those mice. However, we did not observe the dose-dependent increment of parthenogenic activation among different phenotypes (Fig. 3*G*). One possible reason is the dominant negative effect (see *Discussion* below). By the dominant negative effect, the heterozygote itself could cause a 75% reduction of the mature protein. Therefore, we saw a significant increment of parthenogenic activation in the heterozygote. However, only a 25% reduction of mature BMP15 could be generated from the heterozygote to the homozygote. So, we could not see the doubled rate of parthenogenic activation from the homozygote to the heterozygote.

Although identified as a missense variant, the C262T variant only shows in the proprotein and will be removed by proteolytic cleavage after the post-translational processing. Therefore, the variant does not appear in the mature BMP15. However, this variant caused a substantial reduction of mature BMP15 (Fig. 2). One possible mechanism for this reduction of mature and secreted protein is the dominant negative effect. The BMP15 protein exists as a dimer in both proprotein and mature form (35). Therefore, the dominant negative effect can happen at the protein processing stage. Assuming the expression levels of the wild type and the mutant were roughly equal, and the binding affinity between isoforms did not change significantly, then the theoretical ratio of dimerized isoforms in a heterozygote would be WT/WT: WT/MT: MT/MT = 1:2:1. If the penetration rate of the dominant negative effect were 100%, the expected portion of affected protein would be 75%, which is close to the experimental result of 84.7% lost in the mature protein (Fig. 2*A*). The extra reduction could be either experimental error or other mechanism such as decreased processing efficiency due to the cysteine knot. (discussed below).

The C262T mutation will generate a new cysteine at the 88th amino acid residue. So, a new disulfide bond could be created, and the original structure of proprotein could be disrupted. Two in silico predictions suggested the formation of a new disulfide bond between the neo cysteine generated by the C262T variant and the cysteine at position 13. Potentially, the structure of the BMP15 proprotein could be altered, and the posttranslational processing of BMP15 might be affected. This potential alteration in the disulfide bond could be another underlying mechanism for the decreased protein secretion.

Previously, several heterozygous variants of BMP15 affecting the proprotein and leading to reduced secretion of the mature dimer have been identified in primary ovarian insufficiency (POI) patients (36, 37). One possible reason is that BMP15 does not signal only by itself. It is already known that BMP15 can homodimerize or heterodimerize with another TGF-β family member, GDF9. Different dimeric isoforms can exert divergent biological effects by emphasizing different signaling pathways (38). There could be a subtle balance among those signaling pathways transduced by those dimeric isoforms. More importantly, BMP15 forms heterodimers with GDF9 at the proprotein stage. The BMP15 variants in the pro-region may have different degrees of inclination regarding forming individual dimeric isoforms. This differential in the inclination will result in a discrepant ratio of final dimeric isoforms, which can change the balance of the existing signaling and lead to distinct phenotypes. The C262T variant may differ from previous pro-regional variants in the final ratio of different dimeric isoforms and thus result in an alternative phenotype. Another possible reason is that the rareness of OIT (incidence of 3.4×10^{-7}) (1) results in this specific topic was covered in previous studies but not in OIT cases.

Intriguingly, mouse oocyte RNA-sequencing revealed a significant increase in the expression of H-Ras and MEK1 in the C262T carriers. Immunohistochemical staining confirmed the RNA-seq results and revealed more activated MEK1 in the C262T carriers. The Ras/Raf/MEK/ERK (MAPKs) cascade plays essential roles in cell cycle regulation and cell differentiation (39–41) and is an essential cellular signal transduction pathway frequently activated in human cancer (42). However, the most frequent MAPK pathway activation event in carcinomas is *K-Ras* and *B-Raf* mutation. This suggested that a unique signaling pathway is involved in the genesis of OIT. Phenotypically, we also observed that the ovary volume in the variant carriers was approximately two to three times that of wild-type mice at month 6. HE showed that the number of follicles was also significantly increased in variant-carrying mice. Those findings were consistent with the molecular evidence that the MAPK pathway was activated in the ovaries containing the C262T variant.

BMP15 is closely related to the growth and differentiation factor 9 (GDF9). They both belong to the TGF-β superfamily and share the most homologous amino acid sequences. They can form homo and hetero dimers and have a synergistic interaction, and both play critical roles in ovarian functions via paracrine. However, they regulate distinct downstream signaling (43). Under the physiological condition, there is a subtle balance between BMP15 and GDF9 signaling. When the BMP15 level is down, this subtle balance will be broken, and the signal transduced by the GDF9 part will be more dominant. The indirect evidence for this hypothesis is that GDF9 deficiency can result in a decreased ovary size in mice (44), while in our study, the loss of BMP15 will result in an enlarged ovary. This phenotype presumably is mediated by the unevenly higher portion of GDF9 signaling. GDF9 can further activate SMAD2/3 signaling, which, along with SMAD4, can enhance the H-Ras transcription and activate the downstream MAPKs. The above BMP15/GDF9-SMADs-MAPKs signaling can happen in granulosa cells where both BMP15 and GDF9 receptors are expressed. As a potent mitogen, MAPKs strongly stimulate the cell proliferation. The proliferative granulosa cells can lead to an enlarged ovary.

In oocytes, multiple potential mechanisms could activate MAPKs and lead to parthenogenesis. One straightforward possible reason is that the pro-BMP15 could stimulate the oocytes directly. A previous study (45) has shown that pro-BMP15, but not mature BMP15, could significantly enhance the oocyte's developmental

competence, which suggested that pro-BMP15 may also have positive regulatory functions on oocytes. The C262T variant might enhance this positive regulation and lead to parthenogenesis. However, the study was an in vitro experiment and the detailed connecting MAPK part is still missing. Therefore, this hypothesis still needs more exploration. Another explanation is that the unbalanced GDF-9/BMP15 signaling could also affect oocytes just as in the granulosa cells. Receptors for BMP15 are BMPR2 and ALK3/6, and receptors for GDF-9 are BMPR2 and ALK5 (46). It has been documented that BMPR2 and ALK3/6 can be detected in human oocytes (47), while ALK5 was not found in oocytes but in luteinized granulosa cells (48). Accordingly, GDF-9 and BMP15 could compete for the BMPR2 receptor on the oocyte. BMPR2 was consistently expressed at a high level in human preantral follicles yet corresponding GDF-9 and BMP15 levels varied significantly as the follicle grew in size (49). There is a spatiotemporal synergistic regulation of GDF-9, BMP15, and BMPR2 during the development of oocyte and the C262T variant could cause this regulation to unbalanced and thereby activate the downstream MAPKs. However, our work was performed in mice and rodents' oocytes lack a consistent expression of BMPR2 (50) suggesting additional work is also needed to support this mechanism. The third possible mechanism is the interaction between oocytes and the supporting environments. One hypothesis could be the C262T variant causes an unbalanced GDF-9 signal and thereby activates the supporting granulosa cells via paracrine. As feedback, those activated granulosa cells could also secrete other growth factors stimulating an uncontrolled activity of oocytes, such as consistent expression of BMPR2 in oocytes. Just like the previous hypothesis, experimental evidence is still needed.

One limitation of our study is that the exact molecular mechanism by which the BMP15 C262T mutation activates the MAPK pathway needs to be elucidated. Such elucidation is challenging due to the need for experimental materials such as oocyte cell lines and the difficulty of obtaining oocytes. Further studies are needed to validate our hypothesis about MAPK signaling in granulosa cells and oocytes.

Conclusion

In summary, our study showed that OIT could be divided into sporadic and hereditary types and that *BMP15* could be a candidate causal gene for hereditary OIT. The study improved our understanding of the etiology of OIT and provided a potential biomarker for molecular diagnosis and genetic screening for this disorder.

Materials and Methods

Participants. The study participants included two pedigrees of OIT. In pedigree 1, proband III-1 was a 26-y-old with both solid and cystic components in the left ovary that were pathologically diagnosed as OIT grade III. The family medical history indicated that the patient's mother (II-1) was also diagnosed with OIT of the right ovary at 32. The diagnosis of patients III-1 and II-1 was confirmed by pathological re-examination. According to medical records, proband III-1's grandmother (I-1) was also diagnosed with OIT at age 35. Unfortunately, the specimen was not preserved due to the time of collection. In pedigree 2, proband II-3 was a 22-y-old patient with both solid and cystic components on bilateral ovaries. The histological diagnosis showed a grade I immature teratoma on the left and a mature teratoma on the right. A sister of proband II-3 (II-4) was also diagnosed with cystic teratoma in the left ovary and immature teratoma in the right ovary at age 38. All cases showed pathological characteristics typical of OIT.

Five cohorts were used as controls, specifically, 30 patients with sporadic immature teratomas, 50 patients with other ovarian germ cell tumors, 50 patients with epithelial ovarian cancer, 50 patients with ovarian sex cord-stromal tumors, and 50 healthy control women. The study was approved by the Ethics Committee of the Hebei Cancer Institute, and signed informed consent was obtained from all participants.

To investigate the potential genetic causes of the two pedigrees, we performed whole-exome sequencing on members II-1, II-2, III-1, and III-2 of pedigree 1 and members II-1, II-2, II-3, and II-4 of pedigree 2. A variant was considered a candidate if it was present in all affected women and was a rare exonic nonsynonymous variant (minor allele frequency, MAF < 0.0001) in major databases, including the Genome Aggregation (gnomAD), 1000 Genomes Project, and the Exome Sequencing Project (ESP) databases. Another requirement for the candidate mutation was that the variant was predicted to be deleterious and was associated with ovarian function. Variants of interest were amplified by conventional PCR methods and Sanger sequenced using specific primers by Shanghai Generay Biotech Co., Ltd. (https://www.generay.com.cn). Finally, we identified the BMP15 C262T variant as a possible candidate gene for OIT. The BMP15 C262T genotypes of other members of the two pedigrees and control women were determined by Generay Biotech (Shanghai) Co., Ltd. (https://www.generay.com.cn) using Sanger sequencing.

DNA Extraction. Venous blood (5 mL) was collected from each subject into Vacutainer tubes containing EDTA and stored at 4 °C. Genomic DNA was isolated using a standard proteinase K (Merck) digestion followed by a salting out procedure.

Whole-Exome Sequencing. We performed whole-exome sequencing of II-1, II-2, III-1, and III-2 of family 1 and II-1, II-2, II-3, and II-4 members of family 2. Whole-exome capture libraries were prepared from 200ng of genomic DNA with Agilent SureSelect Human All Exon V6 following the manufacturer's protocols and assessed with Agilent 2100 Bioanalyzer High Sensitivity DNA chip. Libraries were sequenced on a NextSeq 6000 sequencer using the High output 300 cycles kit generating 150-bp paired-end single-indexed reads. All libraries were sequenced to an average depth of 100×. Alignment against b37 using Novoalign (version 3.02.08). Variants of interest amplified by conventional PCR methods were assigned to Sanger sequencing using the corresponding primers by Shanghai Generay Biotech Co., Ltd (https://www.generay.com.cn). For each detected variant, the prediction of pathogenicity was assessed using Polyphen2 (https://genetics.bwh.harvard.edu/pph2/), SIFT (http://sift-dna.org), and REVEL (https://sites.google.com/site/revelgenomics/).

Structures Analysis of BMP15 Wild-Type and R88C Mutant. We compared the structures of the mutated BMP15 and the wild-type protein by I-TASSER and PyMOL. The potential new disulfide bonds were predicted using the scratch protein predictor (https://scratch.proteomics.ics.uci.edu/) and Cyscon (https://www.csbio.sjtu.edu.cn/bioinf/Cyscon/).

Construction of BMP15 Expression Plasmids. BMP15 gene variant cDNA was generated using site-directed mutagenesis into the wild-type human BMP15 full-length cDNA, in which the arginine (Arg-88) of wild-type BMP15 was replaced with cysteine. The lentivirus constructs including GV367-empty-MycHis vector (NC-MycHis vector), GV367-wild type BMP15 (WT-MycHis BMP15), and GV367-mutant type BMP15 (MT-MycHis BMP15) were provided by Shanghai GeneChem Company.

Cell Culture. Human embryonic kidney 293T (HEK293T) cells were cultured in DMEM supplemented with 10% FBS, 2 mL-glutamine, penicillin(100U/mL)-streptomycin (0.1 mg/mL). Cells were grown in a humidified chamber at 37 °C with 5% CO_2.

Production of Recombinant BMP15 Proteins. The HEK293T cell suspension was prepared at a density of 3 to 5 × 10^4 cells/mL in a complete medium, followed by inoculating 2 mL per well in a six-well culture plate and incubating at 37 °C for 16 to 24 h until the cell confluence is 50 to 60%. Furthermore, the corresponding virus and infection enhancement solution were added according to the multiplicity of infection (MOI) of 5. The medium in the six-well plate was changed to complete medium 12 h after cell infection. Then, 72 h after cell infection, stable transfectants were selected with 2 μg/mL puromycin (Cayma: Catalog Number13884) and named NC (negative control), WT (wild-type), and MT(mutation-type), respectively. As previously described, positive clones were screened for BMP15 expression by real-time PCR.

In Vitro Molecular Studies. The expression levels of secreted BMP15 proteins between the WT group and the MT group were compared by western blot. Selected HEK293T clones were seeded at a density of 2 × 105 cells/cm^2 and maintained in the medium containing 10% serum. At 70% confluence, cell culture media were switched to no serum media, and the conditioned media were harvested after 72 h. Human recombinant BMP15 proteins were purified from equal amounts of concentrated conditioned media (Becton: Centricon 10,000 Da) at 4 °C.

Then, His Tag Protein Purification Kit (Beyotime P2229s) was used to purify recombinant protein after the concentration of conditioned media. First, 20 μL of well-mixed 50% BeyoGold™ His-tag Purification Resin (denaturing agent type, Beyotime, Shanghai) was added to the concentration media and shaken slowly for 30 min at 4 °C on a shaker to fully bind the target protein with His-tag. Then, the gel was precipitated by centrifugation (1,000 g × 10 s) at 4 °C, 20 μL of the supernatant was retained for subsequent testing, and the rest of the supernatant was discarded. The step was followed by resuspending the gel by adding 100 μL of non-denaturing wash solution, centrifuging at 4 °C (1,000 g × 10 s), taking 20 μL of supernatant to retain for subsequent testing, and discarding the rest of the supernatant. The procedure was repeated for another wash. This washing step was followed by the eluting by adding 20 μL of non-denaturing eluent and gently resuspending the gel. Centrifugation at 4 °C (1,000 g × 10 s) was performed and the supernatant and gel were collected. The supernatant is the target protein with His tag obtained by purification. The elution step was repeated twice. A total of about 60 μL of purified protein sample was collected by elution. The expression of a constitutive protein such as beta-actin was analyzed using the antibody (cell signaling: Catalog Number 8H10D1) to assess the culture media (6 mL per dish) obtained from an equivalent number of cells (1). The amount of recovered protein was evaluated by a colorimetric assay (BCA kit, SEVEN: Catalog Number SW101-02).

Purified proteins from concentrated conditioned media were prepared using 5× loading buffer (250 mM Tris-HCl pH 6.8, 10% SDS, 30% glycerol, 0.02% bromophenol blue) for denaturing nonreducing condition western blot. Purified products from the medium of untransfected HEK293T cells were used as negative control.

Purified proteins were electrophoresed in 4 to 20% MP TGX polyacrylamide gels (BCA kit, SEVEN: Catalog Number SW101-02) and transferred onto PVDF using wet transfer at 300 mAh for 90 min. Five-percent nonfat dry milk in TBST was used to block the membrane for 1 h. Blots were incubated overnight at 4 °C with the anti-MYC antibody (proteintech: Catalog Number 60003-2-Ig) prepared in 1% TBST. After three washes with TBST, the membrane was incubated with Goat anti-Mouse IgG H&L (Abcam: IRDye® 800CW) preadsorbed secondary antibody for 60 min at 37 °C. Following secondary incubation, the blot was washed three times in TBST. β-actin was used as the loading control. Western blots were performed on separate cell-conditioned media at least three times. Band intensity quantification was performed using ImageJ FIJI 2 software (version 2.1.0/1.53C).

H&E Staining and Immunohistochemistry (IHC). Ovarian tissues from the patients with immature ovarian teratomas in two families, patients with immature ovarian teratomas with no family history, and control women were collected and fixed in 4% paraformaldehyde at 4 °C overnight. According to standard techniques, paraffin-embedded tissue sections (4 μm) were stained with hematoxylin and eosin (H&E). Images were taken using a Nikon ECLIPSE Ci (Nikon Instruments, Inc.).

The tissues of the experimental groups mentioned above were collected and fixed in 4% paraformaldehyde at 4 °C overnight. Paraffin-embedded tissue was sectioned continuously with a thickness of 4 mm. Slides were deparaffinized in xylene and rehydrated in graded alcohol. Antigen retrieval was performed in a pressure cooker containing sodium citrate buffer (pH 6.0) for 15 min for all markers. One-percent normal goat serum (ABC Kit VECTA-SIN) was used for closure. The slides were incubated with the primary antibody at 4 °C overnight for BMP15 (rabbit polyclonal antibody to human, Proteintech: Catalog Number18982-1-AP) (1:25). Slides were then incubated with the secondary antibody (biotin-labeled Goat anti-rabbit IgG) and the third antibody (horseradish labeled streptomycin working solution) for 30 min for all antibodies. 3,3′-diaminobenzidine, DAB (Vector ImmPACT DAB) was used as a chromagen for 2 to 3 min, and hematoxylin was used for counterstain. Images were taken using a Nikon ECLIPSE Ci (Nikon Instruments, Inc.).

Animal Care. The research and protocols were approved by the Institutional Animal Care and Use Committee (IACUC) of Hebei Medical University, and all protocols followed the NIH guide for the care and use of laboratory animals (8th edition, 2011, https://www.ncbi.nlm.nih.gov/books/NBK54050). All efforts were made to minimize animal number and suffering. All C57BL/6J mice selected in our experiment were specific pathogen-free (SPF) animals. The feeding environment requires a temperature of 18 to 25 °C, daily temperature difference ≤3 °C, relative humidity of 40 to 70%, fresh air ventilation 10 times per hour, airflow speed ≤0.18 m/s, a pressure difference of 25 Pa, ammonia concentration l5 mg/m^3, noise ≤60dB, illumination of 150 to 300 lux, 12-h light, and 12-h dark. The food and water of mice were SPF grade. The mice were euthanized by carbon dioxide inhalation.

Mouse Model. C57BL/6 mice harboring BMP15 R86C mutation (equivalent to BMP15 R88C in humans) were generated by Cas9/CRISPR-mediated genome editing (Cyagen Biosciences). Briefly, DNA fragment carrying BMP15 targeting gRNA (CCAATCGTGCGGTTCTCCCTTGG) was inserted into the gRNA cloning vector. The oligo donor with targeting sequence, flanked by 124-bp homologous sequences combined on both sides (5′GAGGTACATGCTCAAGTTATACCATCG TTCG GCTGACCCGCATGGCCATCCAAGGGAGAATTGCACGATTGGAGCGAAAATGGTGAGGCTG GTAAAGfCCGTCGGCCAACACAGTAAGGCCTCCC3′) was synthesized (Integrated DNA Technologies). The BMP15 gRNA and Cas9 mRNA were generated by in vitro transcription and co-injected with oligo donor into fertilized eggs.

Generation of New Mouse Line and Genotyping. All new mice were genotyped by Sanger sequencing. The DNAs were extracted from tail-pieces or toes. Interested region in the BMP15 gene was amplified by PCR with primers F:5′GATGTTCTTTGGACTTGGTTAG3′ and R:5′AGTAGCACTCAGTCTTTGTCTTC3′. The DNA sequencing analysis primer was 5′GATGTTCTTTGGACTTGG TTAG3′. Typical sequencing results for each genotype are shown in *SI Appendix*, Fig. S2.

Male mice harboring BMP15 c.C262T mutation allele were mated with WT C57BL/6 female mice to acquire female heterozygous progenies (CT), which were then intercrossed to generate homozygous mutation BMP15 female mice (TT). All mice were maintained in pathogen-free conditions and housed separately during the experiment. Female mice of 4, 8, 12, and 24 wk old were used in this study. Mice that died of unnatural causes during experiments were excluded from the analysis. Animal studies were not blinded. All animal experiments were performed under the approval of the Institutional Animal Care and Use Committee of Hebei Medical University.

Isolation of Mice Oocytes and Spontaneous Parthenogenetic Activation. Oocytes were harvested from mice at 4 wk of age for three different genotypes. Superovulation was induced with an intraperitoneal injection of five international unit (IU) of Pregnant Mare Serum Gonadotropin (PMSG) (Ningbo Sansheng Biological Technology) followed (48 h later) by the injection of 10 IU Human Chorionic Gonadotropin (hCG) (Ningbo Sansheng Biological Technology). The animals were euthanized 17 to 19 h after the hCG injection, and the cumulus-oocyte were collected from the oviducts (by puncturing the swollen ampulla). The complexes were treated with hyaluronidase (150 IU/mL) to remove cumulus cells, and placed in M16 medium, then gassed with 5% CO_2, 5% O_2, and 90% N_2, and incubated at 37 °C for 2 h. Oocytes from five randomly selected mice from each of the three genotypes were used to observe spontaneous parthenogenetic activation. Oocyte morphology was assessed by parthenogenetic activation using a stereomicroscope. There are four classes of parthenogenetic activation. Class I includes oocytes with up to two polar bodies, oocytes produced up to two polar bodies of normal size, and cytoplasm was comparable in size to the normal unfertilized eggs or fertilized eggs at the 1-cell stage. Class II oocytes is characterized with the formation of a pronucleus, Class III oocytes show a typical division. Class IV is the appearance of two cells, two-cell stage embryos with a nucleus in each blastomere (*SI Appendix*, Table S2).

Spontaneous parthenogenetic activation rate of oocytes = (total number of parthenogenetic activated oocytes of four classes/total number of oocytes) × 100%.

Mouse Ovaries Immunohistochemistry. Mouse ovaries were collected and fixed in 4% paraformaldehyde at 4 °C overnight. Paraffin-embedded tissue was sectioned continuously with a thickness of 4 mm. Slides were deparaffinized in xylene and rehydrated in graded alcohol. Antigen retrieval was performed in a pressure cooker containing sodium citrate buffer (pH 6.0) for 15 min for all markers. One-percent normal goat serum (ABC Kit VECTA-SIN) was used for closure. The slides were incubated with the primary antibody at 4 °C overnight for BMP15 (rabbit polyclonal antibody to mouse, Proteintech: Catalog Number18982-1-AP)

(1:25), MEK1 [SZ22-01] (recombinant rabbit monoclonal antibody to mouse, HUABIO: ET1603-20) (1:100), Phospho-MEK1 (S218/S222) [ST0490] (recombinant rabbit monoclonal antibody to mouse, HUABIO: ET1609-50) (1:50), H-Ras (rabbit polyclonal antibody to mouse, GeneTex: GTX116041) (1:25). Slides were then incubated with the secondary antibody (biotin-labeled goat anti-rabbit IgG) and the third antibody (horseradish labeled streptomycin working solution) for 30 min for all antibodies. Images were taken using a Nikon ECLIPSE Ci (Nikon Instruments, Inc.).

Ovary Size Measurements and Follicle Counts. Ovaries from 20 wild-type and 20 CT heterozygous mice at 6 mo of age were collected, respectively. The ovaries were measured with the Vernier caliper and documented (*SI Appendix*, Table S3). The average sizes of ovaries were compared (*SI Appendix*, Fig. S1). After the measurement, ovaries were fixed in formalin, embedded in paraffin, and the sections (typically at the middle part of the ovary) were stained with hematoxylin and eosin (HE). The numbers of follicles at different developmental stages in each slicing section were counted (*SI Appendix*, Table S4). Categorizing of follicles was based on the following rules: primary follicle, one or more layers of granular cells, with the formation of a zona pellucida; secondary follicle, follicle cells appear within the follicle cavity, forming a cumulus, granular cells densely arranged into several layers; mature follicle, the follicular cavity is large and the cumulus is obvious, and the granulosa cells are polygonal, and the radiating crown is formed; atretic follicle, the oocyte structure is unclear, or even disappeared, the zona pellucida shrinks, and the follicle wall collapses.

Mouse Oocyte RNA Sequencing. Oocyte RNAs were sequenced by Shanghai Majorbio Bio-pharm Technology Co., Ltd.

RNA Extraction. Oocytes were separated in the same way as before. Oocytes from 4-wk-old female mice were selected for each genotype, with approximately 140 to 200 oocytes. Total RNA was extracted from the three groups of mouse oocytes using TRIzol® Reagent (Plant RNA Purification Reagent for plant tissue) according to the manufacturer's instructions (Invitrogen), and genomic DNA was removed using DNase I (TaKara). Then, RNA quality was determined by 2100 Bioanalyser (Agilent) and quantified using the ND-2000 (NanoDrop Technologies). Only high-quality RNA sample (OD260/280 = 1.8 ~ 2.2, OD260/230 ≥ 2.0, RIN ≥ 6.5, 28S:18S ≥ 1.0, >1 μg) was used to establish the sequencing library and Nova seq 6000 Sequencing.

Statistical Analysis. All statistical analyses were performed using the Prism program (version 9.0; GraphPad Software). For western blot analysis, the Student's *t* test was used to analyze the difference in secreted protein expression between the WT and MT groups. For analyzing the parthenogenesis activation, one-way ANOVA was used to compare the differences among the three groups, and Tukey's multiple comparisons test was used for inter-group analysis. For immunohistochemical data analysis, the chi-square test was used to compare the differences among the three groups. $*P < 0.05$ was considered significant.

The *t* test (group = 2) or one-way ANOVA (group ≥ 3) was used for the quantitative data, and the chi-square test was used for the qualitative data.

Statement of Translational Relevance. Ovarian immature teratoma (OIT) is a malignant tumor from germ cells with a high malignancy and recurrence rate. It seriously affects young women's physical and mental health and fecundity. The etiology of the disease is unknown so far. Early onset is a noticeable feature of hereditary cancers, and therefore, the disease is suspected to be a malignancy influenced by genetic factors. Previous studies were limited and suggested that the parthenogenesis of oocytes could be the underlying mechanism for this disease. However, this hypothesis still requires to be validated, and the detailed mechanism needs to be elucidated. We identified a potential pathogenic mutation in the BMP15 gene via pedigree studies. Using the genetically engineered animal model, we validated the pathogenicity of this mutation. The spontaneous parthenogenetic activation of oocytes significantly increased in transgenic mice carrying the mutation, and one developed the phenotype of OIT. We also analyzed potential signal pathways via an oocyte-specific transcriptome study. The results suggested that OIT could be classified into hereditary and sporadic types, and BMP15 was a candidate gene for hereditary OIT. This finding improves our understanding of the etiology of OIT. Moreover, the results also implied a potential biomarker for molecular diagnosis, genetic screening, and genetic counseling for high-risk populations.

Ethical Approval Ethical approval was obtained from the Fourth Hospital of Hebei Medical University Research Ethics Committee(No. IACUC-4th Hos Hebmu).

Data, Materials, and Software Availability. All study data are included in the article and/or *SI Appendix*.

ACKNOWLEDGMENTS. We would like to thank Dr. Congrong Liu from the Department of Pathology, School of Basic Medical Sciences, Peking University, and Dr. Yueping Liu from the Department of Pathology of the Fourth Hospital, Hebei Medical University, for their professional help on the pathologies. We also thank Dr. Lei Zhang from the Department of Histology and Embryology, Hebei Medical University, for his assistance in our observation of the development of ovaries. We also thank Dr. Libo Su and Dr. Chang Liu for their help on the animal model. This work is supported by the Natural Science Foundation of Hebei Province, China No. H2020206535

1. H. Smith *et al.*, Incidence and survival rates for female malignant germ cell tumors. *Obstetrics Gynecol.* **107**, 1075–1085 (2006).
2. K. Tewari *et al.*, Malignant germ cell tumors of the ovary. *Obstetrics Gynecol.* **95**, 128–133 (2000).
3. M. B. Heskett *et al.*, Multiregion exome sequencing of ovarian immature teratomas reveals 2N near-diploid genomes, paucity of somatic mutations, and extensive allelic imbalances shared across mature, immature, and disseminated components. *Mod. Pathol.* **33**, 1193–1206 (2020), 10.1038/s41379-019-0446-y.
4. D. Linder, B. K. McCaw, F. Hecht, Parthenogenic origin of benign ovarian teratomas. *N. Engl. J. Med.* **292**, 63–66 (1975).
5. P. Riley, P. Sutton, Ovarian teratomas and genetics of germ-cell formation. *Lancet (London, England)* **1**, 362–363 (1977).
6. W. H. Colledge, M. B. Carlton, G. B. Udy, M. J. Evans, Disruption of c-mos causes parthenogenetic development of unfertilized mouse eggs. *Nature* **370**, 65–68 (1994).
7. N. Hashimoto *et al.*, Parthenogenetic activation of oocytes in c-mos-deficient mice. *Nature* **370**, 68–71 (1994).
8. G. T. O'Neill, M. H. Kaufman, Ovulation and fertilization of primary and secondary oocytes in LT/Sv strain mice. *Gamete Res.* **18**, 27–36 (1987).
9. A. Hampl, J. J. Eppig, Analysis of the mechanism(s) of metaphase I arrest in maturing mouse oocytes. *Development* 121, 925–933 (1995).
10. U. Surti, L. Hoffner, A. Chakravarti, R. E. Ferrell, Genetics and biology of human ovarian teratomas. I. Cytogenetic analysis and mechanism of origin. *Am. J. Hum. Genetics* **47**, 635–643 (1990).
11. D. Linder, Gene loss in human teratomas. *Proc. Natl. Acad. Sci. U.S.A.* **63**, 699–704 (1969).
12. S. W. Faulkner, M. L. Friedlander, Molecular genetic analysis of malignant ovarian germ cell tumors. *Gynecol. Oncol.* **77**, 283–288 (2000).
13. A. Taylor-Weiner *et al.*, Genomic evolution and chemoresistance in germ-cell tumours. *Nature* **540**, 114–118 (2016).
14. S. Shimasaki, R. K. Moore, F. Otsuka, G. F. Erickson, The bone morphogenetic protein system in mammalian reproduction. *Endocr Rev.* **25**, 72–101 (2004).
15. L. Bodin *et al.*, A novel mutation in the bone morphogenetic protein 15 gene causing defective protein secretion is associated with both increased ovulation rate and sterility in Lacaune sheep. *Endocrinology* **148**, 393–400 (2007).
16. S. Fabre *et al.*, Regulation of ovulation rate in mammals: Contribution of sheep genetic models. *Reprod. Biol. Endocrinol.* **4**, 20 (2006).
17. D. Richani, R. B. Gilchrist, The epidermal growth factor network: Role in oocyte growth, maturation and developmental competence. *Hum. Reprod. Update* **24**, 1–14 (2018).
18. R. Rossetti *et al.*, BMP15 mutations associated with primary ovarian insufficiency cause a defective production of bioactive protein. *Hum. Mutat.* **30**, 804–810 (2009).
19. S. G. Kristensen *et al.*, Intrafollicular concentrations of the oocyte-secreted factors GDF9 and BMP15 vary inversely in polycystic ovaries. *J. Clin. Endocrinol. Metabolism* **107**, e3374–e3383 (2022).
20. J. Cheng, A. Randall, M. Sweredoski, P. Baldi, SCRATCH: A protein structure and structural feature prediction server. *Nucleic Acids Res.* **33**, W72–76 (2005).
21. J. Yang, B. He, R. Jang, Y. Zhang, H. Shen, Accurate disulfide-bonding network predictions improve ab initio structure prediction of cysteine-rich proteins. *Bioinformatics (Oxford, England)* **31**, 3773–3781 (2015).
22. J. Saharinen, M. Hyytiäinen, J. Taipale, J. Keski-Oja, Latent transforming growth factor-beta binding proteins (LTBPs)–structural extracellular matrix proteins for targeting TGF-beta action. *Cytokine Growth Factor Rev.* **10**, 99–117 (1999).
23. Y. Hirao, J. J. Eppig, Parthenogenetic development of Mos-deficient mouse oocytes. *Mol. Reprod. Dev.* **48**, 391–396 (1997).
24. W. Thurlbeck, R. Scully, Solid teratoma of the ovary. A clinicopathological analysis of 9 cases. *Cancer* **13**, 804–811 (1960).
25. J. A. Ledermann, Y. Drew, R. S. Kristeleit, Homologous recombination deficiency and ovarian cancer. *Eur. J. (Oxford, England: 1990)* **60**, 49–58 (2016).
26. B. K. McCaw, S. A. Latt, X-chromosome replication in parthenogenic benign ovarian teratomas. *Hum. Genetics* **38**, 253–264 (1977).
27. F. G. Oliveira *et al.*, Evidence of parthenogenetic origin of ovarian teratoma: Case report. *Hum. Reprod.* **19**, 1867–1870 (2004).

28. J. J. Eppig, K. Wigglesworth, D. S. Varnum, J. H. Nadeau, Genetic regulation of traits essential for spontaneous ovarian teratocarcinogenesis in strain LT/Sv mice: Aberrant meiotic cell cycle, oocyte activation, and parthenogenetic development. *Cancer Res.* **56**, 5047–5054 (1996).
29. G. H. Lee *et al.*, Genetic dissection of susceptibility to murine ovarian teratomas that originate from parthenogenetic oocytes. *Cancer Res.* **57**, 590–593 (1997).
30. Q. E. Yang, S. I. Nagaoka, I. Gwost, P. A. Hunt, J. M. Oatley, Inactivation of retinoblastoma protein (Rb1) in the oocyte: Evidence that dysregulated follicle growth drives ovarian teratoma formation in mice. *PLoS Genet* **11**, e1005355 (2015).
31. N. A. Youngson *et al.*, A missense mutation in the transcription factor Foxo3a causes teratomas and oocyte abnormalities in mice. *Mamm. Genome: Off. J. Int. Mamm. Genome Soc.* **22**, 235–248 (2011).
32. H. Peltoketo *et al.*, Female mice expressing constitutively active mutants of FSH receptor present with a phenotype of premature follicle depletion and estrogen excess. *Endocrinology* **151**, 1872–1883 (2010).
33. A. A. Naser *et al.*, MC4R mutant mice develop ovarian teratomas. *Sci. Rep.* **11**, 3483 (2021).
34. Y. Furuta *et al.*, Ovarian teratomas in mice lacking the protooncogene c-mos. *Japanese J. Cancer Res.: Gann* **86**, 540–545 (1995).
35. W. Stocker *et al.*, A variant of human growth differentiation factor-9 that improves oocyte developmental competence. *J. Biol. Chem.* **295**, 7981–7991 (2020).
36. J. Bouilly *et al.*, Identification of multiple gene mutations accounts for a new genetic architecture of primary ovarian insufficiency. *J. Clin. Endocrinol. Metab.* **101**, 4541–4550 (2016).
37. A. Mayer, B. Fouquet, M. Pugeat, M. Misrahi, BMP15 "knockout-like" effect in familial premature ovarian insufficiency with persistent ovarian reserve. *Clin. Genetics* **92**, 208–212 (2017).
38. D. Mottershead *et al.*, Cumulin, an oocyte-secreted heterodimer of the transforming growth factor-β family, is a potent activator of granulosa cells and improves oocyte quality. *J. Biol. Chem.* **290**, 24007–24020 (2015).
39. Y.-Q. Zang, Y.-Q. Zhai, Y.-Y. Feng, X.-Y. Ju, F. Zuo, Molecular mechanisms of quinalizarin induces apoptosis and G0/G1 cell cycle of human esophageal cancer HCE-4 cells depends on MAPK, STAT3, and NF-κB signaling pathways. *Environ. Toxicol.* **36**, 276–286 (2021).
40. F. Fontana *et al.*, δ-Tocotrienol sensitizes and re-sensitizes ovarian cancer cells to cisplatin via induction of G1 phase cell cycle arrest and ROS/MAPK-mediated apoptosis. *Cell Prolif.* **54**, e13111 (2021).
41. D. Cui *et al.*, Epiregulin enhances odontoblastic differentiation of dental pulp stem cells via activating MAPK signalling pathway. *Cell Prolif.* **52**, e12680 (2019).
42. L. S. Steelman *et al.*, JAK/STAT, Raf/MEK/ERK, PI3K/Akt and BCR-ABL in cell cycle progression and leukemogenesis. *Leukemia* **18**, 189–218 (2004).
43. M. Belli, S. Shimasaki, Molecular aspects and clinical relevance of GDF9 and BMP15 in ovarian function. *Vitam. Horm.* **107**, 317–348 (2018).
44. J. Dong *et al.*, Growth differentiation factor-9 is required during early ovarian folliculogenesis. *Nature* **383**, 531–535 (1996).
45. J. Sudiman *et al.*, Bone morphogenetic protein 15 in the pro-mature complex form enhances bovine oocyte developmental competence. *PloS One* **9**, e103563 (2014).
46. H. Chang, J. Qiao, P. Leung, Oocyte-somatic cell interactions in the human ovary-novel role of bone morphogenetic proteins and growth differentiation factors. *Hum. Reprod. Update* **23**, 1–18 (2016).
47. R. Abir *et al.*, Expression of bone morphogenetic proteins 4 and 7 and their receptors IA, IB, and II in human ovaries from fetuses and adults. *Fertil. Steril.* **89**, 1430–1440 (2008).
48. M. Khalaf *et al.*, BMP system expression in GCs from polycystic ovary syndrome women and the in vitro effects of BMP4, BMP6, and BMP7 on GC steroidogenesis. *Eur. J. Endocrinol.* **168**, 437–444 (2013).
49. S. Kristensen *et al.*, Expression of TGF-beta superfamily growth factors, their receptors, the associated SMADs and antagonists in five isolated size-matched populations of pre-antral follicles from normal human ovaries. *Mol. Hum. Reprod.* **20**, 293–308 (2014).
50. J. Juengel, K. McNatty, The role of proteins of the transforming growth factor-beta superfamily in the intraovarian regulation of follicular development. *Hum. Reprod. Update* **11**, 143–160 (2005).